

Effect of the background flow on the motility induced phase separation

Soni D. Prajapati,¹ Akshay Bhatnagar,^{2,*} and Anupam Gupta^{1,†}

¹*Department of Physics, Indian Institute of Technology Hyderabad, Hyderabad 502284, India*

²*Department of Physics, Indian Institute of Technology Palakkad, Palakkad 678623, Kerala, India.*

We simulate active Brownian particles (ABPs) with soft-repulsive interactions subjected to a four-roll-mill flow. In the absence of flow, this system exhibits motility-induced phase separation (MIPS). To investigate the interplay between MIPS and flow-induced mixing, we introduce dimensionless parameters: a scaled time, τ , and a scaled velocity, v , characterizing the ratio of ABP to fluid time and velocity scales, respectively. The parameter space defined by τ and v reveals three distinct ABP distribution regimes. At low velocities $v \ll 1$, flow dominates, leading to a homogeneous mixture. Conversely, at high velocities $v \gg 1$, motility prevails, resulting in MIPS. In the intermediate regime ($v \sim 1$), the system's behavior depends on τ . For $\tau < 1$, a moderately mixed homogeneous phase emerges, while for $\tau > 1$, a novel phase, termed flow-induced phase separation (FIPS), arises due to the combined effects of flow topology and ABP motility and size. To characterize these phases, we analyze drift velocity, diffusivity, mean-squared displacement, giant number fluctuations, radial distribution function, and cluster-size distribution.

Keywords: Active Brownian Particles, MIPS, Four-roll-mill flow

I. INTRODUCTION

Active matter systems consist of entities that continuously consume energy from their environment to induce internal changes, typically resulting in directed motion [1, 2]. These systems represent a subset of non-equilibrium systems observed across various length scales in nature, from the microscopic (e.g., bacteria [3, 4], sperm cells) to the macroscopic (e.g., fish [5], birds [6, 7], animals [8, 9], and humans [10]). To gain deeper insights into these systems, researchers have developed and studied numerous synthetic active particles in controlled laboratory environments, including Janus particles [11], vibrating beds of self-propelling particles [12], active droplets [13], and robotic systems [14, 15]. Due to underlying interactions among the constituent entities of active systems, these systems exhibit emergent phenomena. Prominent examples include motility-induced phase separation (MIPS) [16, 17], characterized by density fluctuations arising from self-propulsion, flocking, or herding behavior displaying collective polar order [18], and the emergence of nematic (apolar) ordering due to intrinsic anisotropy in the system components [12].

Active systems typically coexist with surrounding fluids, as exemplified by bacterial colonies [3, 4], active colloids [11], and fish schools [5]. However, the influence of the underlying flow on the emergent behavior of these systems remains largely unexplored. This study aims to elucidate how background flow affects the formation and characteristics of MIPS.

MIPS can be observed in various active particle models, including Active Ornstein-Uhlenbeck particles [19], Active Brownian Particles (ABPs) [16, 17, 20], and run-and-tumble particles [21, 22]. Despite model variations,

these systems exhibit qualitatively similar phase separation behavior. In this study, we employ ABPs with soft repulsion and no alignment to simulate microorganisms in a fluid environment. System dynamics in the absence of flow agrees with previous findings [16, 17]. We are always in the parameter regime where we observe MIPS without background flow. MIPS displays distinct characteristics compared to equilibrium phase separation, including reduced diffusivity and drift [17], giant number fluctuations (with standard deviation ΔN scaling nearly linearly with mean particle number N) [12, 23], ordered packing in the dense phase [24], and a bimodal cluster size distribution [24, 25]. This work investigates how these features are modified by the introduction of background flow

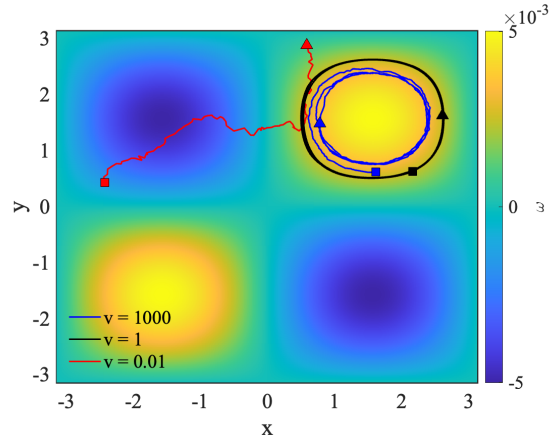


FIG. 1: Representative Trajectories of ABPs with $\tau = 0.05$ and $\phi = 0.7$ for three scaled-velocities overlaid on the vorticity field corresponding to four-roll-mill flow. The triangle and the square represent the starting and ending points of the trajectories, respectively.

Since this is the first attempt to address such questions,

* Correspondence: akshayb@iitpkd.ac.in

† Correspondence: agupta@phy.iith.ac.in

we begin by considering a controlled flow, a four-roll-mill flow [26, 27] (Fig. 1). This flow exhibits a clear distinction between vortical and strain-dominated regions. Known for its efficiency in mixing passive scalars [28, 29], this flow creates a competition with the demixing tendency inherent to MIPS. To quantify the relative importance of flow and particle motility, we introduce dimensionless parameters based on velocity and time scales: the scaled velocity $v = \frac{v_p}{u_f}$ and scaled time $\tau = \frac{\omega_f}{\nu_r}$. Here, v_p and $1/\nu_r$ represent the characteristic velocity and time scales of the ABPs, while (u_f) and $(1/\omega_f)$ correspond to those of the flow. Our analysis explores the dynamics within the v - τ parameter space.

II. MODEL AND SIMULATIONS

We consider a collection of N interacting ABPs, confined to two dimensions, and suspended in a fluid. The ABPs are modeled as disks of radius a , each propelled with a self-propulsion velocity v_p along the orientation vector $\hat{\mathbf{p}}_i$, where i ranges from 1 to N . In two dimensions, $\hat{\mathbf{p}}_i$ is expressed as $(\cos(\theta_i), \sin(\theta_i))$, with θ_i denoting the angle between the orientation vector of the i -th particle and the x -axis. The equations of motion, for the particle with position, \mathbf{r}_i are as follows:

$$\dot{\mathbf{r}}_i = v_p \hat{\mathbf{p}}_i + \mu_t \sum_{j \neq i} \mathbf{F}_{ij} + \boldsymbol{\eta}_i^T(t) + \mathbf{u}(\mathbf{r}_i, t), \quad (1a)$$

$$\dot{\theta}_i = \eta_i^R(t) + \frac{1}{2}\omega(\mathbf{r}_i, t), \quad (1b)$$

where, \mathbf{F}_{ij} models the soft repulsive interaction between the i -th and j -th particle and is given as $\mathbf{F}_{ij} = -k(2a - |\mathbf{r}_{ij}|)\hat{\mathbf{r}}_{ij}$, if $|\mathbf{r}_{ij}| < 2a$, otherwise, it is 0. μ_t is the motility of an ABP. $\boldsymbol{\eta}_i^T(t)$ and $\eta_i^R(t)$ are translational and rotational noise, respectively. They obey a Gaussian distribution with zero mean and auto-correlation functions $\langle \boldsymbol{\eta}_{i\alpha}(t) \boldsymbol{\eta}_{j\beta}^T(t') \rangle = 2D\delta_{ij}\delta_{\alpha\beta}\delta(t - t')$ and $\langle \eta_i^R(t) \eta_j^R(t') \rangle = 2\nu_r\delta_{ij}\delta(t - t')$, where, $D = k_B T \mu_t$ is translational diffusivity, ν_r is the rotational diffusivity, k_B is Boltzmann constant, T is the temperature of the background fluid, and α, β represent cartesian components. In this work, we have neglected the translational noise to isolate the impact of rotational noise. \mathbf{u} and ω represent the velocity and vorticity fields of the background flow, respectively.

We solve 2D incompressible Navier-Stokes equation(NSE) to mimic the background flow in which ABPs are moving. We use stream function-vorticity formulation of NSE: [30]

$$\partial_t \omega + \mathbf{u} \cdot \nabla \omega = \nu \nabla^2 \omega - \mu \omega + \mathbf{f}_\omega; \quad \nabla^2 \psi = \omega; \quad (2)$$

where, $\psi(\mathbf{r}_i, \mathbf{t})$ and $\omega = \nabla \times \mathbf{u}(\mathbf{x}, \mathbf{t}) \equiv \omega \hat{\mathbf{z}}$, is the stream function and vorticity field, respectively, in two dimensions and $\hat{\mathbf{z}}$ is a unit vector normal to the fluid film. ν

is kinematic viscosity and μ Ekman-friction [30–32]. We take roll-mill form for the external forcing, \mathbf{f}_ω [26, 27],

$$\mathbf{f}_\omega = f_0 \sin(k_f x) \sin(k_f y) \hat{\mathbf{z}} \quad (3)$$

where, f_0 is the amplitude of the forcing and k_f is the forcing wave vector. For large viscosity limit (small Re), we know the exact solution of the NSE, i.e. $(u_x, u_y) = \frac{f_0}{4\nu k_f^3} (-\sin(k_f x) \cos(k_f y), \cos(k_f x) \sin(k_f y))$. The corresponding vorticity field is shown in Fig. 1.

We use a square box $[0, 2\pi]^2$ with periodic boundary conditions(PBCs) for background flow and particle dynamics. The square box is uniformly discretized in 512^2 grid point. In our numerical simulation, we use the pseudo-spectral method to solve NSE (2) on these grid points to describe the dynamics of background flow [30–32]. Runge-Kutta method of 2nd order is used for time marching. We use $k_f = 1$, $\nu = 1$, $\mu = 0$ which produces a four-roll-mill flow, i.e., pairs of clockwise and anti-clockwise vortices separated by small regions dominated by strain [33] (see Fig. 1). This flow has been studied both experimentally and theoretically for the mixing of passive tracers [28, 29].

We use bilinear interpolation to determine flow properties at particle positions. Equations (1a) and (1b) are solved for $N = 3518$ ABPs, corresponding to a packing fraction $\phi = 0.7$, to assess particle dynamics in the background flow using the Euler-Maruyama method [34, 35]. The packing fraction is defined as $\phi = \frac{N\pi \times a^2}{L^2}$. We have chosen $\phi = 0.7$ because this ϕ value shows MIPS in the absence of background flow [17]. We have kept $\mu_t = 100$ and $k_f = 1$. We are not taking into account the back-reaction of the ABPs on the flow. All quantitative results presented in this manuscript pertain to three sets of self-propulsion velocities and three sets of rotational diffusivities. The characteristic fluid vorticity $\omega_f = 0.005$, which gives three scaled times $\tau = 400.0 (\gg 1)$, $1.00 (\sim 1)$, and $0.05 (\ll 1)$. The characteristic fluid velocity $u_f = 0.0018$ which gives three scaled velocity $v = 1000, 1, \& 0.01$.

III. RESULTS

We observe three distinct spatial distributions of ABPs across the considered ranges of τ and v . (a) Clustering of ABPs due to MIPS ($v \gg 1$): In this regime, the ABP velocity significantly exceeds the characteristic flow velocity, resulting in ABP motility dominating the dynamics and leading to MIPS. (b) Clustering due to flow topology; flow-induced phase separation (FIPS) ($v \sim 1 \& \tau > 1$), and (c) a homogeneously mixed phase ($v \ll 1$). We illustrate these different phases of ABP distribution through a $\tau - v$ phase space (Fig. 3). Subsequent subsections detail qualitative and quantitative comparisons with the corresponding case without background flow.

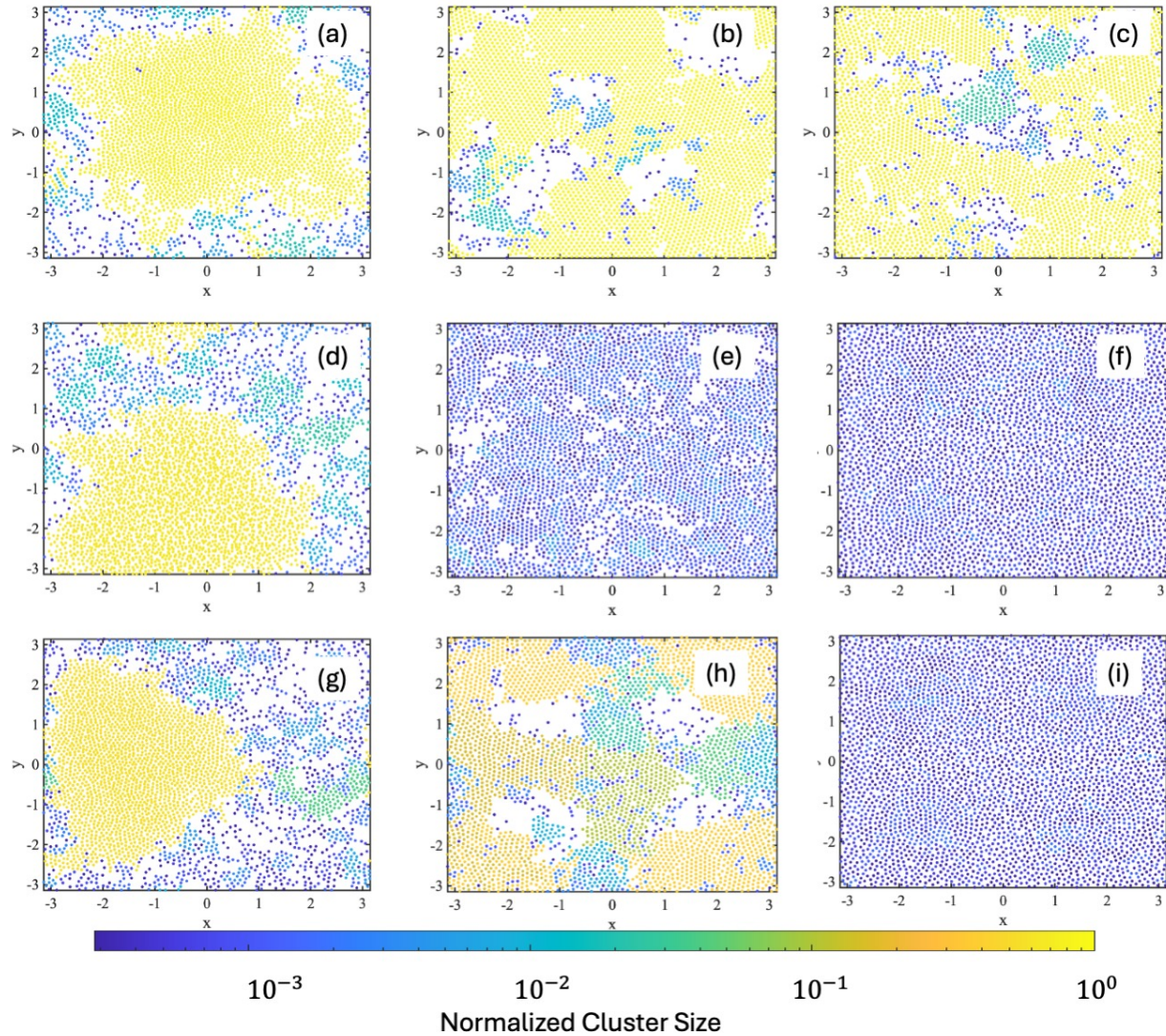


FIG. 2: Representative snapshot of ABPs with $\phi = 0.7$ for three different scaled-velocities $v = 1000$ (left column), 1 (middle column), and 0.01 (right column); and no background flow with $\nu_r = 0.005$ (top row), scaled time $\tau \sim 1$ with background flow (middle row), scaled time $\tau \sim 400$ with background flow (bottom row). The color codes represent the normalized size of the cluster.

A. Phase separation of ABPs

In the absence of background flow, a dense suspension ($\phi \gtrsim 0.4$) of interacting ABPs exhibits the well-known phenomenon of MIPS [16, 17]. The top row of Fig. 2 shows snapshots of particle positions for three different self-propulsion velocities v_p : 1000 (panel (a)), 1 (panel (b)), and 0.01 (panel (c)). In all cases, $\phi = 0.7$ and ν_r is fixed at 1.25×10^{-5} .

When a background (roll-mill) flow is introduced to these suspensions, we observe that MIPS persists for cases with large scaled velocity (i.e., $v \gg 1$), regardless of the scaled time τ . This is shown in the panels (d) and (g) of Fig. 2 for $\tau \simeq 1$ and $\tau = 400$, respectively. In this

regime, the background flow acts as a small perturbation to the dynamics of ABPs, evident from the red trajectory shown in Fig. 1, and MIPS is still dominant. When we decrease the scaled velocity v by decreasing the self-propelled velocity v_p and making it comparable to the fluid velocity scale ($v \sim 1$), we observe that the clustering is dependent on the scaled time τ . When scaled time $\tau \leq 1$ we observe a weak clustering phase as shown in Fig. 2(e). For $\tau > 1$, we observe a phase-separated state different from MIPS. The flow topology drives this clustering and all the ABPs try to cluster themselves in the strain-dominated region, i.e., the region with Okubo-Weiss parameter $\Lambda < 0$ as shown in Fig. 2(h). One can observe in Fig. 1 that the blue trajectory is slowly drift-

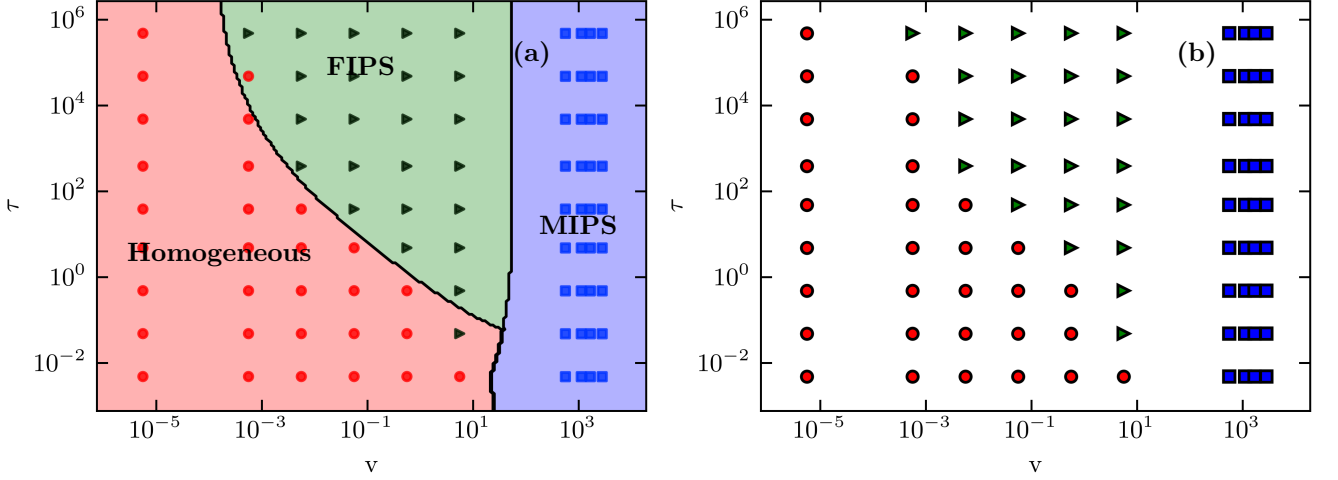


FIG. 3: (a) Phase diagram of ABPs spatial distribution in τ - v plane for $\phi = 0.7$. Three different phases — homogeneous phase (red region), flow-induced phase separation (FIPS) (green region), and motility-induced phase separation (MIPS) (blue region) — are observed. The dots represent actual simulations and the shaded background corresponds to best-fit predictions for regime boundaries using support vector machines (SVM). (b) \mathcal{O} in the τ - v plane. Red circles correspond to homogeneous phase ($\mathcal{O} = 1$), green triangles corresponds to FIPS phase ($\mathcal{O} = 2$) and blue square correspond to MIPS phase ($\mathcal{O} = 0$)

ing away from the vortex core and towards the strain-dominated region. Okubo-Weiss parameter is defined as $\Lambda = \frac{\omega^2 - \sigma^2}{8}$ [31, 36], $\Lambda > 0$ and < 0 represent vortical and strain-dominated regions, respectively, where $\sigma^2 \equiv \sum_{ij} \sigma_{ij} \sigma_{ij}$ (strain rate), and $\sigma_{ij} \equiv \partial_i u_j + \partial_j u_i$, i, j are cartesian-indices. It is important to note that we observe this type of clustering only when the velocity of ABPs and background flow are comparable and $\tau \gg 1$. Since, $\tau \gg 1$, the persistence length for ABPs is large compared to the vortical structures (half of the box size in this case) of the flow, and once these particles reach the strain-dominated region, which are straight paths for this flow, tend to stay in this region. If the ABPs are in the vortical region, due to the long persistence length of the ABPs, they exit the rotating vortical regions and are pushed to the strain-dominated region. This clustering is due to the flow topology and the finite size of the ABPs, so we define this clustering behavior as flow-induced phase separation (FIPS). When we further decrease the scaled velocity $v \ll 1$, the mixing due to the roll-mill flow starts to dominate, and we see the system in the homogeneous phase, for both τ values as shown in Figs. 2(f) and 2(i).

We have observed that the system's state — MIPS, FIPS, or homogeneous phase — depends on the scaled velocity v and scaled time τ . To elucidate this further, we conducted a parameter scan in τ - v space (Fig. 3). For small τ , systematically increasing v transitions the system from a homogeneous state (red region) to a MIPS state (blue region). Upon exceeding $\tau = 1$, a new phase-separated state, FIPS (green region), emerges. The v range exhibiting FIPS expands with increasing τ . At extremely large v , only MIPS is observed. Within the FIPS

regime, most ABPs reside in strain-dominated regions where $\Lambda < 0$. We can characterize $\bar{\Lambda} \equiv 1/N \sum_i \langle \Lambda_i \rangle_t$ for ABPs in the steady state, where $\langle \cdot \rangle_t$ represents time average. Based on the sign of $\bar{\Lambda}$ we can determine whether a regime in FIPS ($\bar{\Lambda} < 0$) or MIPS/homogeneous ($\bar{\Lambda} > 0$) (Fig. 9(a)).

In MIPS dominated regime, we do not expect any correlation between the flow velocity and the ABP velocity. So if we estimate the $\hat{\mathbf{u}} \cdot \hat{\mathbf{v}} \equiv \frac{1}{N} \sum_i \langle \frac{\mathbf{u}(\mathbf{r}_i, t) \cdot \mathbf{v}_i}{|\mathbf{u}(\mathbf{r}_i, t)| |\mathbf{v}_i|} \rangle_t$, it will be close to zero in the MIPS regime and close to 1 for the homogeneous regime. $\hat{\mathbf{u}} \cdot \hat{\mathbf{v}}$ will maintain an intermediate value for FIPS regime (Fig. 9(b)). Hence, by combining the above information we can define the following order parameter: $\mathcal{O} = \Theta(-\bar{\Lambda}) + \Theta(\hat{\mathbf{u}} \cdot \hat{\mathbf{v}} - \epsilon)$, where ϵ is a threshold value that we have chosen to be 0.02 to differentiate the $\hat{\mathbf{u}} \cdot \hat{\mathbf{v}}$ value from MIPS to the rest of the regimes. Fig. 3(b) shows \mathcal{O} in τ - v plane. $\mathcal{O} = 0$ (blue square) corresponds to the MIPS regime, as both the terms in the \mathcal{O} will not contribute. $\mathcal{O} = 1$ (red circles) corresponds to the homogeneous regime, as only the second terms in the \mathcal{O} will contribute. $\mathcal{O} = 2$ (green triangles) corresponds to the FIPS regime, as both the terms in the \mathcal{O} will contribute. In Fig. 3(b) we can observe different values of order parameter \mathcal{O} for different phases similar to Fig. 3(a) where different phases are marked with different colors based on the distribution of particles.

B. Mean Square Displacement (MSD)

For interacting ABPs, the mean-square displacement (MSD) is given by [17]

$$\langle [\Delta \mathbf{r}(t)]^2 \rangle = 4D_e \left[t + \frac{1}{\nu_r} (e^{-\nu_r t} - 1) \right], \quad (4)$$

where $D_e = v_0^2/2\nu_r$ is the effective diffusivity and v_0 is effective drift velocity; for non-interacting ABPs $v_0 = v_p$.

In Fig. 4 we show the MSD for ABPs, where the solid (dashed) lines are for the case with (without) background flow. As expected, for $t \ll \nu_r^{-1}$, there is ballistic behavior with $\langle [\delta \mathbf{r}(t)]^2 \rangle \sim v_0^2 t^2$, whereas at later time, the diffusive behavior with $\langle [\delta \mathbf{r}(t)]^2 \rangle \sim 4D_e t$ is observed. The time of cross-over from ballistic to diffusive regime is defined as transition time T_{trans} . We show the MSD for three scaled-times $\tau \ll 1$ (Fig. 4(a)), $\tau \sim 1$ (Fig. 4(b)) & $\tau \gg 1$ (Fig. 4(c)). Each panel shows the plots for three scaled-velocities $v \gg 1$ (red), ~ 1 (blue), $\gg 1$ (black). We observe that for the case without background flow, the transition time $T_{\text{trans}} \simeq \nu_r^{-1}$, marked by vertical magenta lines, whereas for the case with background flow, the T_{trans} is v dependent. For large v , T_{trans} is independent of background flow (red-solid curve) as MIPS drives the dynamics. For $v \ll 1$ (Fig. 4 black-solid curve), since the major contribution to the velocity of the ABPs is the background flow, T_{trans} is dependent on the fluid time scale, marked by the brown vertical lines. T_{trans} for the FIPS case (blue-solid curve) follows a similar trend as $v \ll 1$ case, with a slight delay. An important point to note is that the MSDs for FIPS and mixed-phase display a bump before going to the diffusive regime. This bump is associated with the fact that the ABPs in this regime follow the streamlines and move in quasi-closed orbits. The bump for the mixed phase is stronger as they follow the closed orbits for a relatively longer time, attributed to their low motility Fig. 1. A similar bump is observed in MSD for the non-interacting ABPs [37], attributed to the trapping effect due to the vortices of the roll-mill flow.

Drift velocity.- Using eq. 4, in the limit $t \ll T_{\text{trans}}$ we extract the drift velocity v_0 from MSD (Figure 5(a)). In Fig. 5(a), we show that plot of drift velocity v_0 vs scaled velocity v . The drift velocities for the case without background flow (dashed curves) go together for different values of τ , as there is no perturbation from the background flow $\Rightarrow v_0 \sim v_p$, as can be seen in Fig. 5(a), the dashed straight lines with slope 1, for $\tau \sim 0.05, 1 \& 400$. Once we introduce the background flow (solid curves), we see that for $v < 1$ the fluid velocity dominates, and the drift velocity of ABPs is comparable to fluid velocity u_f . This behaviour is independent of τ , and v_0 remains comparable to u_f till v approaches unity. For large v the drift velocity again becomes comparable to the v_p .

Diffusivity.- Similarly, using eq. 4, in the limit $t \gg T_{\text{trans}}$, we extract diffusivity D_e from MSD. In Fig. 5(b) we show the plot of diffusivity D_e vs scaled velocity v . The diffusivity for the case without background flow

(dashed curves) follows $v_0^2/2\nu_r$, maintains a slope '2' and a gap of the ratio of the time scales, i.e., ~ 400 between black and blue and ~ 20 between blue and red curves. In the presence of background flow, when $v \ll 1$, the diffusivity is completely controlled by the background flow and it becomes independent of τ . As v starts to approach unity, we observe that the diffusivity curves start to bifurcate for different τ values and approach the value corresponding to the without background flow. Finally, curves merge with their counterparts in the absence of background flow for $v \gg 1$.

C. Giant number fluctuation

In the phase separating active systems, we expect to observe giant number fluctuations as $\Delta N = N^\alpha$, where α can be as large as 1 for non-equilibrium systems in two-dimensions [17, 38, 39]. Here N and ΔN represent the average and variance, respectively, of the number of ABPs within a subdomain of size l^2 . We find that, in the absence of background flow, for all values of v and τ , the slope α approaches 1 (dashed curves), indicative of a clear phase-separated state (Fig 6). In the phase-separated MIPS region for scaled velocity $v \gg 1$ we observe $\alpha \sim 1$ (red-solid curve), similar to the case without background flow (red dashed curves). In the FIPS region (the green region in Fig. 3), where $v \sim 1 \& \tau \gg 1$ we find $0.5 < \alpha < 1$ (solid-blue curve in Fig 6). Here, ABPs form clusters in strain-dominated regions, but the clustering is less pronounced than in the MIPS regime, leading to α values between 0.5 and 1. In the mixed-phase (red region in Fig. 3) where $v \ll 1$, α is approximately 0.5, here ABPs are following the background flow and the exponent corresponds to an equilibrium state.

D. Radial Distribution Function

To understand the packing behavior of ABPs in different regimes of the phase space (Fig. 3), we calculate the radial distribution function (RDF) as shown in Fig. 7. In the MIPS region, where $v \gg 1$, ABPs within large clusters exhibit close packing with local hexagonal order, as evident in the first and second peaks at $2a$, $2\sqrt{3}a$, respectively, of the RDF (Fig. 7(a) and (b), red solid lines) [40]. The peaks are broader owing to the softness of the ABPs. In the FIPS region, characterized by $v \sim 1$ and $\tau \gg 1$, the RDF displays peaks at $2a$ and $4a$, with a smaller peak at $2\sqrt{3}a$ (Fig. 7(b), blue curve). This intermediate peak suggests transient hexagonal packing due to the clustering in the strain-dominate regions of the flow. In contrast, the homogeneously mixed region, defined by $v \ll 1$ (Fig. 7, black curve) or $v \sim 1$ and $\tau \leq 1$ (Fig. 7(a), blue curve), exhibits RDF peaks at $2a$ and $4a$, indicative of a lack of ordered packing among the ABPs.

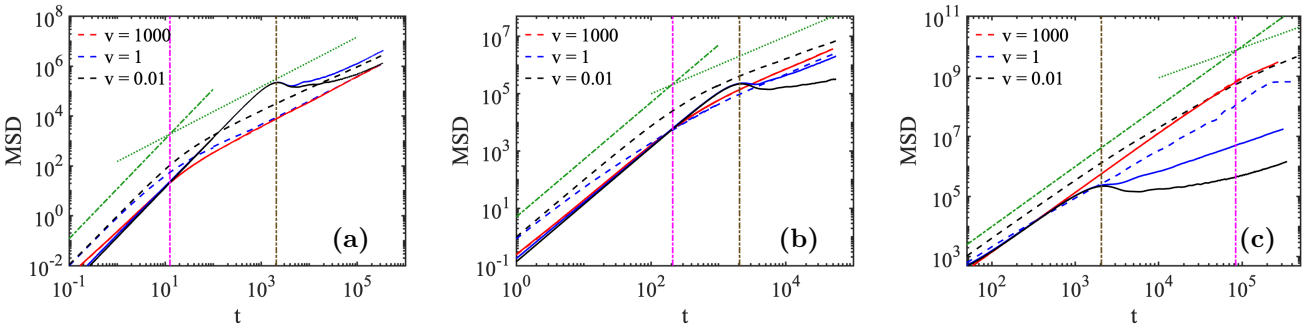


FIG. 4: Mean-square displacement (MSD) of ABPs versus time with $\phi = 0.7$ and for scaled-time (a) $\tau \sim 0.05$, (b) $\tau \sim 1$ & (c) $\tau \sim 400$. Solid (dashed) lines indicate MSD with (without) background flow for three different scaled velocities $v = 1000$ (red curve), 1 (blue curve), & 0.01 (black curve). The green dashed-dotted (dotted) line shows the slope 2 (1) on a log scale, a guide to the eyes for a diffusive (ballistic) regime. Their intersection shows the transition time T_{trans} from ballistic to diffusive regime. The magenta and brown dashed-dotted brown vertical lines represent the rotational diffusion time scale ($1/\nu_r$) and fluid time scale ($2\pi/\omega_f$), respectively. To bring MSDs for different v on the same y-scale, we rescale the MSDs by $1/v_0^2$ for MIPS cases and by $1/u_f^2$ for FIPS and homogeneous cases.

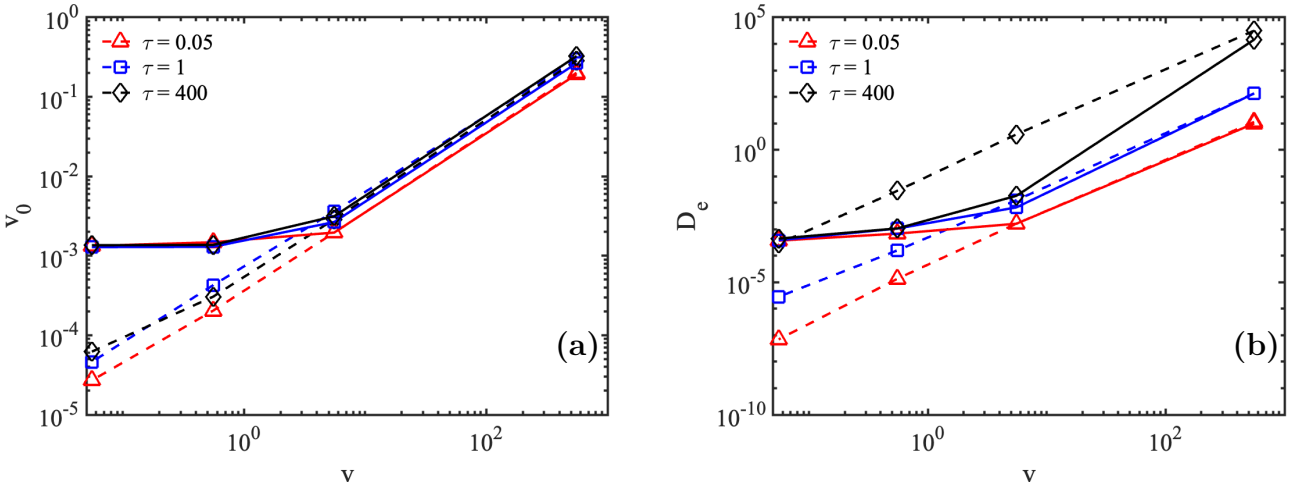


FIG. 5: (a) Drift velocity (v_0) and (b) Diffusivity (D_e) of ABPs versus scaled velocity v with $\phi = 0.7$ for three different scaled times $\tau \sim 0.05$ (red), ~ 1 (blue), ~ 400 (black). Solid (dashed) lines indicate with (without) background flow.

E. Clusters Size Distribution

After understanding packing, we focused on the size of the cluster and its distribution in a statistically steady state. In Fig. 8, we have plotted the normalized cluster size distribution (CSD) $P(n)/P(1)$ vs cluster size n , where $P(n)$ is the probability of finding a cluster of size ' n ' ABPs. Irrespective of the parameter space, normalized CSD fits a power law with exponential cut-off $P(n)/P(1) \simeq 1/n^\beta \exp(-n/n_0)$ [25], we observe β to be around 2. In the MIPS region, where $v \gg 1$ (red curve), we observe a bimodal distribution of cluster-size n (Fig. 8(a-b)), which is similar to the observation for standard MIPS [24, 25]. The bimodal distribution is a signature of the clear phase separation and it is also observed for the FIPS region (blue curve, Fig. 8(b)). For

$v \ll 1$ (black curve) and $v \sim 1$ & $\tau \sim 1$ (blue curve, Fig. 8(a)), CSD shows an unimodal power-law decay, latter with a larger β (slower decay). The slow decay (shown by the dashed yellow line with $\beta = 2.1$, a guide to the eye), can be attributed to the formation of moderately large clusters, in comparison to the case with $v \ll 1$. Additionally, for $\tau \sim 1$ (Fig. 8(a)), CSD shows a non-monotonous power-law exponent β as a function of v , whereas for $\tau \gg 1$ (Fig. 8(b)) CSD shows no significant dependence of v on β .

IV. CONCLUSION

We investigated the dynamics of interacting ABPs with and without background flow in two dimensions. We have used a four-roll mill flow, as a background

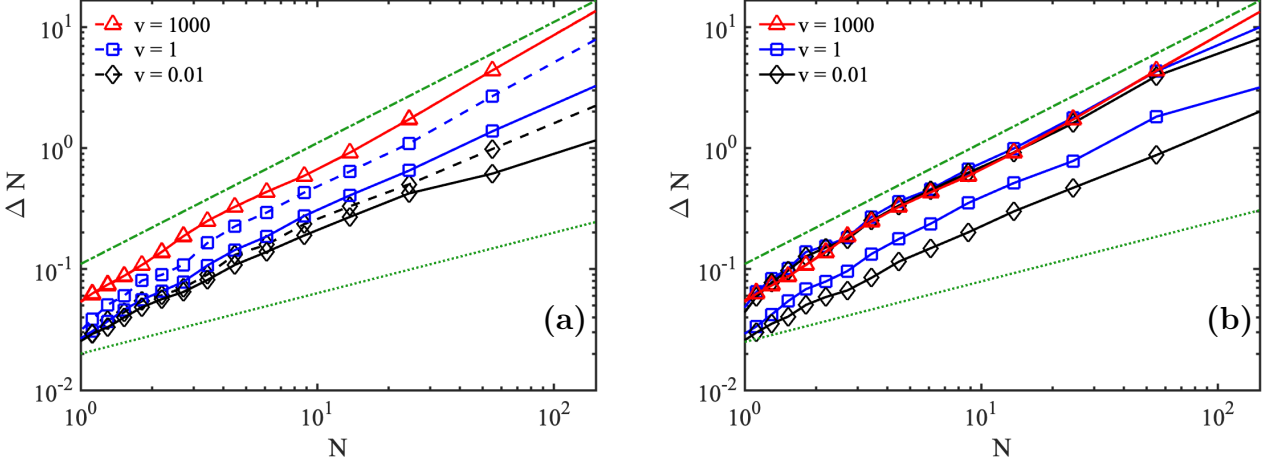


FIG. 6: Standard deviation of fluctuations ΔN versus average number N of ABPs in subsystem of size $l = \sqrt{\pi a^2 N / \phi}$ for scaled-time (a) $\tau \sim 1$ & (b) $\tau \sim 400$. Solid (dashed) lines are for ABPs with (without) background flow for three different scaled velocities $v = 1000$ (red curve), 1 (blue curve), & 0.01 (black curve). The green dashed-dotted (dotted) line denotes $\Delta N = N$ ($\Delta N = N^{\frac{1}{2}}$).

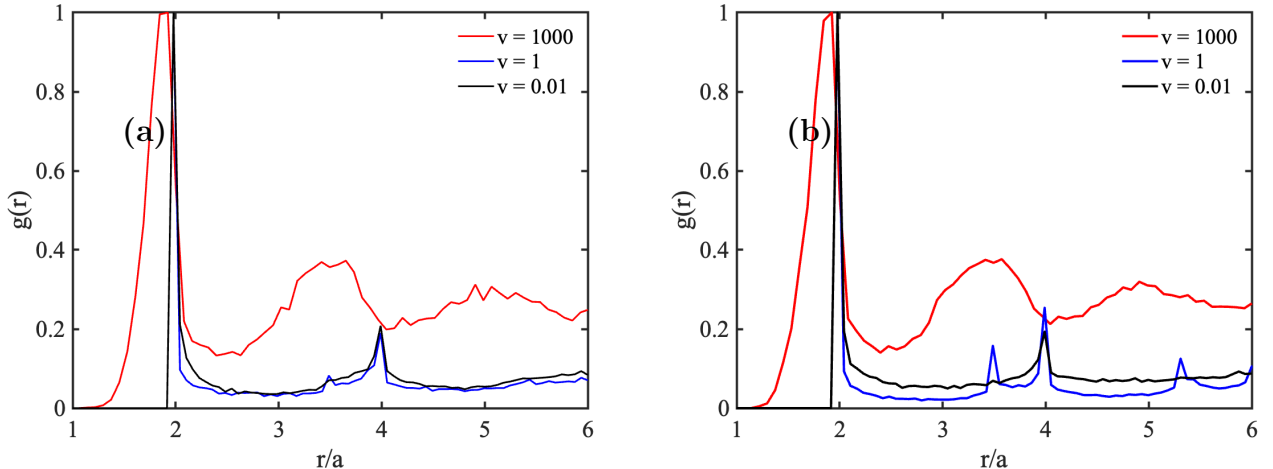


FIG. 7: Radial distribution function (RDF) $g(r)$ versus r/a of ABPs for fixed $\phi = 0.7$, for three different scaled velocities $v = 1000$ (red curve), 1 (blue curve), & 0.01 (black curve) with scaled time (a) $\tau \sim 1$ and (b) $\tau \sim 400$.

flow, where the topology remains fixed in space with distinct vortical and strain-dominated regions. While previous studies on non-interacting self-propelled particles in this flow revealed strong clustering only for anisotropic particles [33], our results demonstrate that isotropic ABPs with steric repulsion exhibit clustering under certain parameter regimes (Fig. 3). We identify three distinct phases based on particle spatial distribution: homogeneous, flow-induced phase separation (FIPS), and motility-induced phase separation (MIPS). The phase diagram in Fig. 3 reveals precise control over these phases through the scaled velocity (v) and scaled persistence time (τ). A novel phase, FIPS, emerges for $\tau > 1$ and $v \sim 1$, characterized by clustering in the strain-

dominated region, distinct from MIPS. This FIPS phase occupies a narrow region in the parameter space, as illustrated in Fig. 3.

In the MIPS phase, ABPs exhibit no correlation with flow characteristics. Conversely, in the FIPS phase, they respond to flow topology and correlate with flow velocity. The homogeneous phase displays a strong correlation with flow velocity but no discernible correlation with flow topology. Based on these observations, we introduced an order parameter that distinguishes between the three phases by adopting distinct values in each regime.

To quantitatively differentiate the phases, we analyzed drift velocity, diffusivity, mean squared displacement (MSD), giant number fluctuations, radial distribu-

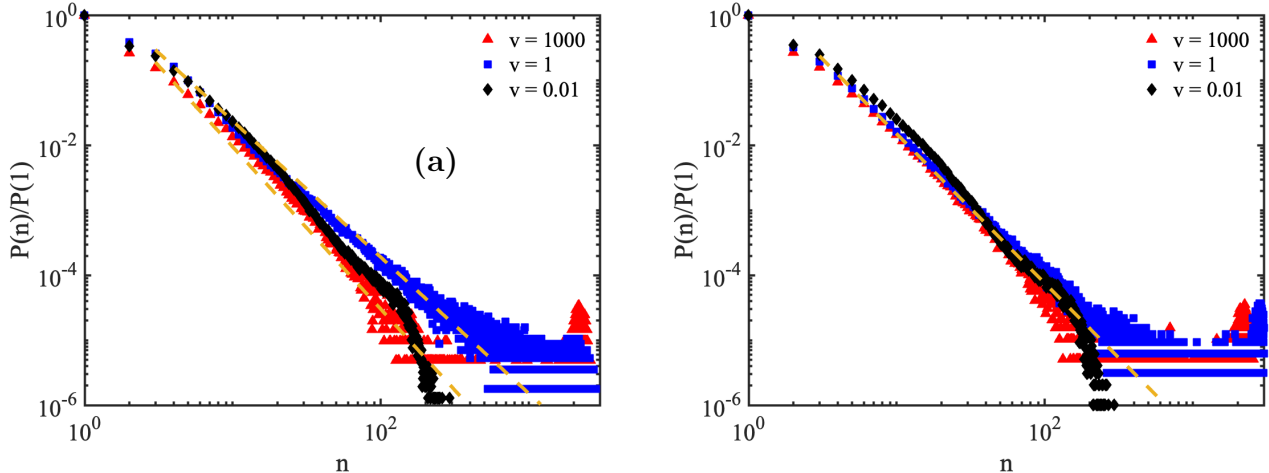


FIG. 8: Cluster size distribution (CSD) $P(n)/P(1)$ versus n where n is the cluster size for ABPs for fixed $\phi = 0.7$, for three different scaled velocities $v = 1000$ (red triangles), 1 (blue squares), & 0.01 (black diamonds) with scaled time (a) $\tau \sim 1$ and (b) $\tau \sim 400$. Two yellow dashed lines in (a) guide the eyes with the slopes -2.1 & -2.5 respectively, and a yellow dashed line in (b) guide the eyes with the slope -2.3 .

tion function (RDF), and cluster size distribution. MSD revealed ballistic behavior at early times and diffusive behavior at later times. The nature of the transition from ballistic to diffusive regime and the transition time T_{trans} depend on the region of the $\tau - v$ parameter space. For MIPS, a smooth transition occurred at the rotational diffusion timescale of ABPs. In contrast, FIPS and homogeneous phases exhibited a bump after the transition due to quasi-closed ABP trajectories (Fig. 1), with T_{trans} determined by the flow timescale. Flow in FIPS and homogeneous phases control drift velocity and diffusivity, whereas in the MIPS phase, they are controlled by self-propulsion and rotational diffusion of ABPs. The exponent α of giant number fluctuation ($\Delta N \propto N^\alpha$) decreased monotonically from 1 to 0.5 transitioning from MIPS to FIPS to homogeneous phase. RDF analysis indicated hexagonal closed packing for MIPS, disordered packing for the homogeneous phase, and an intermediate packing with both ordered and disordered features for FIPS. Cluster size distribution showed bimodal behavior for MIPS and FIPS, contrasting with the unimodal power-law decay of the homogeneous phase.

In this study, hydrodynamic interactions were neglected to isolate the effect of background flow on MIPS. Previous studies have demonstrated that hydrodynamic interactions and boundary conditions can induce a clustered phase for these motile swimmers, a phenomenon also described as flow-induced phase separation [41]. This type of phase separation has been observed in various systems, including polymers in elongated flow [42], and phase separation of wormlike micelles, a ‘living’ polymeric system, in flow [43].

Natural microorganisms reside in fluid environments and often display non-uniform spatial distributions [44, 45]. In active matter systems, where interactions between constituents play a crucial role, such non-uniformity can be attributed to MIPS. However, in certain scenarios, these spatial heterogeneities can originate from external flow conditions [44, 45]. This study investigates the combined effect of these mechanisms. To the best of our knowledge, this work represents the first exploration of the impact of background flow on MIPS. Our study reveals a novel phase, flow-induced phase separation (FIPS), distinct from MIPS. The proposed mechanism for FIPS is straightforward and readily adaptable to experimental settings. We anticipate that this research will stimulate further investigations into the effects of background flow on MIPS.

V. ACKNOWLEDGMENT

AG acknowledges the funding from SERB-India (grant no. MTR/2022/000232, grant no. CRG/2023/007056-G); DST-India (grant no. DST/NSM/R&D HPC Applications/2021/05 and grant no. SR/FST/PSI-309 215/2016).

VI. APPENDIX: OKUBO-WEISS PARAMETER AND VELOCITY CORRELATION

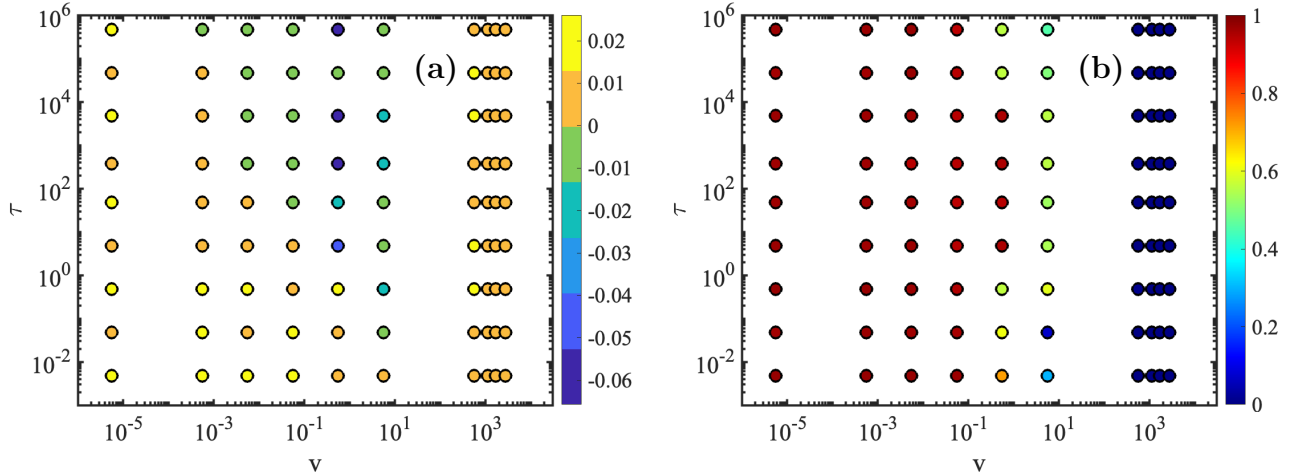


FIG. 9: (a) $\bar{\Lambda}$ and (b) $\hat{\mathbf{u}} \cdot \hat{\mathbf{v}}$ values of ABPs in the τ - v plane for $\phi = 0.7$. Colorbars indicate magnitude. The FIPS regions (top middle in the left panel) exhibit negative $\bar{\Lambda}$ values, while the MIPS regions (extreme right in the right panel) show $\hat{\mathbf{u}} \cdot \hat{\mathbf{v}}$ values close to zero.

[1] M. C. Marchetti, J.-F. Joanny, S. Ramaswamy, T. B. Liverpool, J. Prost, M. Rao, and R. A. Simha, Hydrodynamics of soft active matter, *Reviews of modern physics* **85**, 1143 (2013).

[2] C. Bechinger, R. Di Leonardo, H. Löwen, C. Reichhardt, G. Volpe, and G. Volpe, Active particles in complex and crowded environments, *Reviews of Modern Physics* **88**, 045006 (2016).

[3] Y. Wu, A. D. Kaiser, Y. Jiang, and M. S. Alber, Periodic reversal of direction allows myxobacteria to swarm, *Proceedings of the National Academy of Sciences* **106**, 1222 (2009).

[4] A. Sokolov, M. M. Apodaca, B. A. Grzybowski, and I. S. Aranson, Swimming bacteria power microscopic gears, *Proceedings of the National Academy of Sciences* **107**, 969 (2010).

[5] E. Crosato, L. Jiang, V. Lecheval, J. T. Lizier, X. R. Wang, P. Tichit, G. Theraulaz, and M. Prokopenko, Informative and misinformative interactions in a school of fish, *Swarm Intelligence* **12**, 283 (2018).

[6] M. Nagy, Z. Ákos, D. Biro, and T. Vicsek, Hierarchical group dynamics in pigeon flocks, *Nature* **464**, 890 (2010).

[7] T. Mora, A. M. Walczak, L. Del Castello, F. Ginelli, S. Melillo, L. Parisi, M. Viale, A. Cavagna, and I. Giardina, Local equilibrium in bird flocks, *Nature physics* **12**, 1153 (2016).

[8] C. L. Hueschen, A. R. Dunn, and R. Phillips, Wildebeest herds on rolling hills: Flocking on arbitrary curved surfaces, *Physical Review E* **108**, 024610 (2023).

[9] A. Garcimartín, J. Pastor, L. Ferrer, J. Ramos, C. Martín-Gómez, and I. Zuriguel, Flow and clogging of a sheep herd passing through a bottleneck, *Physical Review E* **91**, 022808 (2015).

[10] N. Bellomo, D. Clarke, L. Gibelli, P. Townsend, and B. Vreugdenhil, Human behaviours in evacuation crowd dynamics: From modelling to “big data” toward crisis management, *Physics of life reviews* **18**, 1 (2016).

[11] H.-R. Jiang, N. Yoshinaga, and M. Sano, Active motion of a janus particle by self-thermophoresis in a defocused laser beam, *Physical review letters* **105**, 268302 (2010).

[12] V. Narayan, S. Ramaswamy, and N. Menon, Long-lived giant number fluctuations in a swarming granular nematic, *Science* **317**, 105 (2007).

[13] R. Dey, C. M. Buness, B. V. Hokmabad, C. Jin, and C. C. Maass, Oscillatory rheotaxis of artificial swimmers in microchannels, *Nature communications* **13**, 2952 (2022).

[14] K. P. O’Keeffe, H. Hong, and S. H. Strogatz, Oscillators that sync and swarm, *Nature communications* **8**, 1504 (2017).

[15] S. Paramanick, A. Pal, H. Soni, and N. Kumar, Programming tunable active dynamics in a self-propelled robot, *The European Physical Journal E* **47**, 34 (2024).

[16] G. S. Redner, M. F. Hagan, and A. Baskaran, Structure and dynamics of a phase-separating active colloidal fluid, *Physical Review Letters* **110**, 055701 (2013).

[17] Y. Fily and M. C. Marchetti, Athermal phase separation of self-propelled particles with no alignment, *Physical Review Letters* **108**, 1 (2012).

[18] T. Vicsek, A. Czirók, E. Ben-Jacob, I. Cohen, and O. Shochet, Novel type of phase transition in a system of self-driven particles, *Physical review letters* **75**, 1226 (1995).

[19] D. Martin and T. A. de Pirey, Aoup in the presence of brownian noise: a perturbative approach, *Journal of Statistical Mechanics: Theory and Experiment* **2021**, 043205 (2021).

[20] M. Sanoria, R. Chelakkot, and A. Nandi, Influence of interaction softness on phase separation of active particles, *Physical Review E* **103**, 052605 (2021).

[21] T. Bertrand, Y. Zhao, O. Bénichou, J. Tailleur, and R. Voituriez, Optimized diffusion of run-and-tumble particles in crowded environments, *Physical Review Letters*

120, 198103 (2018).

[22] I. Santra, U. Basu, and S. Sabhapandit, Run-and-tumble particles in two dimensions: Marginal position distributions, *Physical Review E* **101**, 062120 (2020).

[23] J. Toner, Y. Tu, and S. Ramaswamy, Hydrodynamics and phases of flocks, *Annals of Physics* **318**, 170 (2005).

[24] M. Sanoria, R. Chelakkot, and A. Nandi, Percolation transition in phase-separating active fluid, *Physical Review E* **106**, 034605 (2022).

[25] P. Dolai, A. Simha, and S. Mishra, Phase separation in binary mixtures of active and passive particles, *Soft Matter* **14**, 6137 (2018).

[26] P. Gutierrez-Castillo and B. Thomases, Proper orthogonal decomposition (pod) of the flow dynamics for a viscoelastic fluid in a four-roll mill geometry at the stokes limit, *Journal of Non-Newtonian Fluid Mechanics* **264**, 48 (2019).

[27] J. S. Lee, R. Dylla-Spears, N. P. Teclamariam, and S. J. Muller, Microfluidic four-roll mill for all flow types, *Applied physics letters* **90** (2007).

[28] T. Solomon and I. Mezić, Uniform resonant chaotic mixing in fluid flows, *Nature* **425**, 376 (2003).

[29] T. Solomon and J. P. Gollub, Chaotic particle transport in time-dependent rayleigh-bénard convection, *Physical Review A* **38**, 6280 (1988).

[30] R. Pandit, D. Banerjee, A. Bhatnagar, M. Brachet, A. Gupta, D. Mitra, N. Pal, P. Perlekar, S. S. Ray, V. Shukla, *et al.*, An overview of the statistical properties of two-dimensional turbulence in fluids with particles, conducting fluids, fluids with polymer additives, binary-fluid mixtures, and superfluids, *Physics of fluids* **29** (2017).

[31] A. Gupta, P. Perlekar, and R. Pandit, Two-dimensional homogeneous isotropic fluid turbulence with polymer additives, *Physical Review E* **91**, 033013 (2015).

[32] A. Gupta, D. Vincenzi, and R. Pandit, Elliptical tracers in two-dimensional, homogeneous, isotropic fluid turbulence: The statistics of alignment, rotation, and nematic order, *Physical Review E* **89**, 021001 (2014).

[33] C. Torney and Z. Neufeld, Transport and aggregation of self-propelled particles in fluid flows, *Physical review letters* **99**, 078101 (2007).

[34] K. Malakar, A. Das, A. Kundu, K. V. Kumar, and A. Dhar, Steady state of an active brownian particle in a two-dimensional harmonic trap, *Physical Review E* **101**, 022610 (2020).

[35] G. Janzen and L. M. Janssen, Aging in thermal active glasses, *Physical Review Research* **4**, L012038 (2022).

[36] P. Perlekar, S. S. Ray, D. Mitra, and R. Pandit, Persistence problem in two-dimensional fluid turbulence, *Physical review letters* **106**, 054501 (2011).

[37] L. Caprini, F. Cecconi, A. Puglisi, and A. Sarracino, Diffusion properties of self-propelled particles in cellular flows, *Soft Matter* **16**, 5431 (2020).

[38] S. Henkes, Y. Fily, and M. C. Marchetti, Active jamming: Self-propelled soft particles at high density, *Physical Review E* **84**, 040301 (2011).

[39] S. Ramaswamy, R. A. Simha, and J. Toner, Active nematics on a substrate: Giant number fluctuations and long-time tails, *Europhysics Letters* **62**, 196 (2003).

[40] J. P. Singh, S. Pattanayak, S. Mishra, and J. Chakrabarti, Effective single component description of steady state structures of passive particles in an active bath, *The Journal of Chemical Physics* **156** (2022).

[41] S. Thutupalli, D. Geyer, R. Singh, R. Adhikari, and H. A. Stone, Flow-induced phase separation of active particles is controlled by boundary conditions, *Proceedings of the National Academy of Sciences* **115**, 5403 (2018).

[42] M. H. Nafar Sefiddashti, B. J. Edwards, and B. Khomami, Flow-induced phase separation and crystallization in entangled polyethylene solutions under elongational flow, *Macromolecules* **53**, 6432 (2020).

[43] P. D. Olmsted, Dynamics and flow-induced phase separation in polymeric fluids, *Current opinion in colloid & interface science* **4**, 95 (1999).

[44] W. M. Durham, J. O. Kessler, and R. Stocker, Disruption of vertical motility by shear triggers formation of thin phytoplankton layers, *Science* **323**, 1067 (2009).

[45] W. M. Durham, E. Climent, M. Barry, F. De Lillo, G. Boffetta, M. Cencini, and R. Stocker, Turbulence drives microscale patches of motile phytoplankton, *Nature communications* **4**, 2148 (2013).